THE JOURNAL OF BIOLOGICAL CHEMISTRY VOL. 285, NO. 32, pp. 24420–24431, August 6, 2010

Pannexin1 and Pannexin2 Channels Show Quaternary Similarities to Connexons and Different Oligomerization Numbers from Each Other*[S]

Received for publication, February 18, 2010, and in revised form, May 21, 2010 Published, JBC Papers in Press, June 1, 2010, DOI 10.1074/jbc.M110.115444

Cinzia Ambrosi[‡], Oliver Gassmann[§], Jennifer N. Pranskevich[‡], Daniela Boassa[‡], Amy Smock[‡], Junjie Wang[¶], Gerhard Dahl[¶], Claudia Steinem[§], and Gina E. Sosinsky[‡‖1]

From the [‡]National Center for Microscopy and Imaging Research and the [‖]Department of Neurosciences, University of California San Diego, La Jolla, California 92093-0608, the [§]Institute for Organic and Biomolecular Chemistry, University of Göttingen, Tammannstrasse 2, 37077 Göttingen, Germany, and the [¶]Department of Physiology and Biophysics, University of Miami, School of Medicine, Miami, Florida 33136

Pannexins are homologous to innexins, the invertebrate gap junction family. However, mammalian pannexin1 does not form canonical gap junctions, instead forming hexameric oligomers in single plasma membranes and intracellularly. Pannexin1 acts as an ATP release channel, whereas less is known about the function of Pannexin2. We purified cellular membranes isolated from MDCK cells stably expressing rat Pannexin1 or Pannexin2 and identified pannexin channels (pannexons) in single membranes by negative stain and immunogold labeling. Protein gel and Western blot analysis confirmed Pannexin1 (Panx1) or Pannexin2 (Panx2) as the channel-forming proteins. We expressed and purified Panx1 and Panx2 using a baculovirus Sf9 expression system and obtained doughnut-like structures similar to those seen previously in purified connexin hemichannels (connexons) and mammalian membranes. Purified pannexons were comparable in size and overall appearance to Connexin46 and Connexin50 connexons. Pannexons and connexons were further analyzed by single-particle averaging for oligomer and pore diameters. The oligomer diameter increased with increasing monomer molecular mass, and we found that the measured oligomeric pore diameter for Panxs was larger than for Connexin26. Panx1 and Panx2 formed active homomeric channels in *Xenopus* oocytes and *in vitro* vesicle assays. Crosslinking and native gels of purified homomeric full-length and a C-terminal Panx2 truncation mutant showed a banding pattern more consistent with an octamer. We purified Panx1/Panx2 heteromeric channels and found that they were unstable over time, possibly because Panx1 and Panx2 homomeric pannexons have different monomer sizes and oligomeric symmetry from each other.

Pannexins (Panxs),[2] connexins (Cxs), and innexins belong to one superfamily (1). Panxs (Pan in ancient Greek means "whole") were given this name because of their presumptive ubiquitous presence in multicellular animals (2). Although the term "pannexin" can encompass invertebrate forms, the mammalian branch commonly known as pannexins is formed by three members: Panx1, Panx2, and Panx3. In rat, Panx1 contains 426 amino acids (~48 kDa), Panx2 has 674 amino acids (~70 kDa), and Panx3 has 392 amino acids (~44.7 kDa). There is very high conservation of amino acid sequence within individual Panx isoforms among mammalian species compared with between Panx1, Panx2, and Panx3. Panx1 is ubiquitously expressed, whereas Panx2 has expression only in the central nervous system. Panx3 has a different pattern of expression from Panx1 and Panx2. Panx3 is found in mouse skin, osteoblasts, and specialized cartilage (3, 4).

Several studies have addressed the function of pannexins in tissue, particularly with respect to the role it plays in purinergic receptor signaling. As part of this pathway, Panx1 may release large signaling molecules like ATP and arachidonic derivatives and as a result may be involved in astrocytic Ca^{2+} wave propagation via P_2X_7 receptors (5, 6). Panx1 has also been implicated in ischemic, excitotoxic, and ATP-dependent cell death (7) and is part of the immunological and neuronal inflammasome (8–10). The function of Panx2 in the central nervous system remains unknown. The role of Panx3 in tissues remains to be established because it has not been shown to be functional by itself or in combination with Panx1 or Panx2 in electrophysiological assays (11) but has been shown to express at the plasma membrane in tissue culture cells (3).

Based on membrane topology folding and secondary structure prediction, Panxs were first proposed to form gap junction-like structures (12). More recent results established that

* This work was supported, in whole or in part, by National Institutes of Health Grants GM072881 and GM065937 (to G. E. S.) and GM048610 (to G. D.). This work was also supported by National Science Foundation Grant MCB0543934 (to G. E. S.) and the European Union within the framework of the Marie Curie Training Network 019335 Translocation (to C. S.) and by Bundesministerium für Bildung und Forschung Grant 13N9110 (to C. S.). Most of this work was conducted at the National Center for Microscopy and Imaging Research at San Diego, which is supported by National Institutes of Health Grant RR04050.

[S] The on-line version of this article (available at http://www.jbc.org) contains supplemental Figs. S1–S3.

[1] To whom correspondence should be addressed: National Center for Microscopy and Imaging Research, University of California, San Diego, School of Medicine, BSB 1070, 9500 Gilman Dr., MC 0608, La Jolla, CA 92093-0608. Tel.: 858-534-0128; Fax: 858-534-7497; E-mail: gsosinsky@ucsd.edu.

[2] The abbreviations used are: Panxs, pannexin; EM, electron microscopy; Panx1, pannexin1; Panx2, pannexin2; Panx3, pannexin3; Cx, connexin; WT, wild type; CBX, carbenoxolone; MDCK, Madin-Darby canine kidney; BSA, bovine serum albumin.

although Cxs and Panxs share a number of topological similarities, there are also important differences. One is that their sequence composition is very different from connexins. Four conserved cysteines are present in the pannexin extracellular loops rather than six as for connexins. These cysteines may influence the formation and properties of gap junction channels (13). Our group and others established that pannexins have glycosylation sites on their extracellular loops and are found in glycosylated forms in various cell types (3, 14, 15). Studies showed that although connexons become coupled very soon after incorporation into the membrane (16), the active function for Panx1 pannexons is in nonjunctional membranes (3, 15, 17–19). Both Panx1 homomeric pannexons and Panx1/Panx2 heteromeric pannexons are expressed at the plasma membrane (20). The Panx1/Panx2 heteromeric combination as well as Panx1 homomeric pannexons have been reported to make functional pannexons and gap junction-like channels in single and paired *Xenopus* oocytes, respectively (11, 21). However, although functional Panx1 channels have been found in tissues, Panx1 and Panx2 have not been seen to co-localize and form heteromeric Panx1/Panx2 channels at the tissue level. Thus, pannexins represent a novel class of connexin-like channel proteins. Because others and our group have found that Panx channels do not typically form gap junctions, to avoid confusion we distinguish between pannexons (single membrane oligomers of Panxs), connexons (single membrane hexamers of Cxs, also referred to as "hemichannels"), and gap junction channels (double membrane paired hexamers of Cxs).

In this study, we analyzed purified Panx1 and Panx2 channels (pannexons) by coordinated biochemical analysis and electron microscopy of mammalian membranes and as purified pannexons from baculovirus infected insect cells and compared them with Cxs connexons. Also, included are functional assays for Panx1 and Panx2, showing that Panx2 does form active channels as homomeric channels. We studied the oligomeric state of Panx2 and found that it most likely forms octamers as opposed to Panx1, which we previously established forms hexamers (15). Furthermore, we purified Panx1 and Panx2 heteromeric channels but found that they are unstable, probably because of the different symmetries that we see in homomeric channels and the consequent mismatch between the two isoforms.

EXPERIMENTAL PROCEDURES

Antibodies—Panx1 and Panx2 antibodies were generated against peptides using sequences in the N terminus (Panx1 monoclonal), intracellular loop (Panx2 polyclonal), and the C terminus (Panx2 polyclonal) and custom produced and purified by Abgent, Inc. (San Diego). The full design and characterization of these antibodies are described.[3] We also used two antibodies from Invitrogen: mouse monoclonal anti-His_6 tag antibody (catalogue numbers R930-25 or R931-25) and a mouse monoclonal for Cx26 that is directed against a cytoplasmic loop epitope (catalogue number 13-8100).

Generation of Constructs for Mammalian and Baculovirus Expression—All of the constructs in this paper use amino acid sequences found in rat pannexins or rat connexins except Cx50 (mouse). Rat cDNAs encoding wild type rat Panx1 and Panx2 were originally and kindly provided by Dr. Roberto Bruzzone. Madin-Darby canine kidney (MDCK) cells were maintained at 37 °C and 10% CO_2 in Dulbecco's modified Eagle's medium containing 10% fetal bovine serum. Another longer rat Panx2 construct was also generated according to the sequence found in Ref. 22. Development and characterization of Panx1-Myc and Panx2-HA mammalian cell lines are described in Ref. 15.[3] The experiments were conducted on stably expressing cell lines in selection with the antibiotic hygromycin.

Connexin (rCx26, rCx43, rCx46, and rCx46) and pannexin (rPanx1 and rPanx2) gene sequences were cloned into the baculovirus vector pBlueBac4.5 using XbaI and HindIII as restriction sites with a V5 epitope/hexahistidine (V5-His_6) added to the C terminus. Isolation and purification of baculovirus expressed Sf9 proteins are described in Ref. 23. The truncation mutant for Panx2 was designed by first running secondary structure predictions on the Panx2 C terminus from three or four different Internet available algorithms from the ExPASy proteomics server to look for commonalities of α-helices, β-sheets, and random coil in the Panx2 C terminus among the five different algorithms: NNPredict (24), GOR (25), SCRATCH (26), PSIPRED (27), and JPRED (28). Truncations are done in random coil sequence sections with a distance intermediate to any predicted consensus, consecutively ordered secondary structure (α-helices or β-strands).

Gap Junction and Connexon/Pannexon Purifications—Gap junction preparations were purified from HeLa cells stably expressing rCx26 wild type (rCx26WT) (29), and we used the same protocol to obtain Panx1 and Panx2 membranes from MDCK stably expressing rPanx1 or rPanx2. Pannexons or connexons were isolated from baculovirus-infected Sf9 cells according to our published methods using a His_6 tag affinity purification protocol (23, 30, 31). Purified proteins were negatively stained with 2% uranyl acetate for EM visualization and analysis. Western blots were performed using denaturing 4–12% SDS gel PAGE as we previously published (23). The gels were stained using either a silver staining kit or a SYPRO Ruby gel stain (Invitrogen, Inc.). Buffer exchange was performed using Amicon Microcon centrifugal filter devices YM-100 (Millipore, Temecula, CA).

Cross-linking of Pannexons—After purification in insect cells, the proteins were cross-linked using 300 μg/ml DSP for 30 min at room temperature. If the sample was meant for electrophoresis, the reaction was stopped by the addition of glycine following the protocol used in Ref. 15.

Immunogold Labeling Membranes on Grids—A 5-μl drop of isolated membranes in solution was placed on carbon-coated grids and allowed to adsorb for approximately 1 min at room temperature. The grids were then dipped into BSA-Tris buffer drops (20 mM Tris-HCl, pH 8, 1 mg/ml BSA) plus 5% goat serum for 30 min. After that they were dipped in primary solution (BSA-Tris buffer +1% goat serum + primary antibody) for 1 h. The Panxs and Cx26 primary antibodies were diluted 1:50 or 1:100. The grids were washed by plunging them in three

[3] D. Boassa, A. Papas, and G. E. Sosinsky, manuscript in preparation.

drops of BSA-Tris buffer and then incubated in secondary solution (BSA-Tris buffer +1% goat serum + 10 nm gold-conjugated secondary) for ~30 min. Secondary dilutions were 1:50. Finally the grids were washed in three drops of double distilled water and negatively stained with 2% uranyl acetate.

Immunogold Labeling Membranes in Cross-section by Thin Section EM—The membranes were spun down for 10 min at 18,3000 relative centrifugal force at room temperature. Then the pellet was resuspended in the BSA-Tris buffer described in the previous section and again collected by centrifugation. The pellet was resuspended in primary solution (primary diluted 1:1 or 1:2 with BSA-Tris buffer) and incubated for 1 h at room temperature. The membranes were then collected by centrifugation and resuspended in the BSA-Tris buffer. This wash procedure was performed two more times, and then the membrane was resuspended in the secondary solution containing secondary 10-nm gold conjugated antibody (diluted 1:1 or 1:2 with BSA-Tris buffer) and incubated for 1 h at room temperature. Three washes were then performed using BSA-Tris buffer. For both labeled and unlabeled membrane preparations analyzed by thin section EM, the membranes were collected by centrifugation, and the membrane pellet was fixed for 30 min in fixing solution (2% glutaraldehyde, 1% tannic acid, pH 7–8, 0.1 M cacodylate buffer) at room temperature. The pellet was washed three times with cacodylate buffer diluted 1:3 and stained in ice for 1 h with 2% osmium tetroxide (diluted with cacodylate buffer) and then stained with 2% uranyl acetate in the same conditions. Following standard protocols, the dark pellet was dehydrated on ice with an increasing ratios of ethanol:water, followed by two changes of 100% ethanol. The pellet was then embedded in Durcupan resin for sectioning and EM analysis.

Electron Microscopy—High dose, conventional transmission electron microscope images were recorded on a JEOL 1200 electron microscope operated at 80 kV. Thin sections were 80 nm thick and counterstained with lead. The specimens were negatively stained with 1 or 2% uranyl acetate. A 200-kV FEI Sphera microscope was used to image the negatively stained grids in low doses (15–20 $e^-/Å^2$) at 40,000 magnification. The images were recorded on film, scanned with Nikon LS-9000 digital film scanner and processed using EMAN1/EMAN2 using standard procedures for image alignment and averaging (32).

Cytochrome c-loaded Vesicle Permeability Assay—This protocol follows that used in several studies (33–36). Pannexons were reconstituted into vesicles using ~1 nmol of purified pannexin. The vesicles were prepared in 1 ml of aqueous solution containing 50 mM KCl, 20 mM Tris, pH 7.4, 22 mg of *n*-octyl-β-glucopyranoside, 6 mg of cytochrome *c*, and 10 mg of 1-palmitoyl-2-oleoyl-*sn*-glycero-3-phosphocholine. The protein-lipid-detergent solution was mixed and incubated for 30 min at 4 °C followed by detergent removal using Biobeads SM overnight at 4 °C. The formed proteoliposomes with an average diameter of 200 nm were applied to a Sephadex G-75 column to separate free cytochrome *c* from the cytochrome *c*-loaded proteoliposomes. The fractions were collected and analyzed at 417 and 630 nm using a UV-visible spectrophotometer. The cytochrome *c*-loaded proteoliposomes were collected in the void volume. Control vesicles without pannexons but with enclosed cytochrome *c* were prepared in parallel. Sodium ascorbate was used to reduce the intraliposomal cytochrome *c*, which was monitored at 417 nm using a UV-visible spectrophotometer. A 200-μl vesicle aliquot was added to 790 μl of buffer (50 mM KCl, 20 mM Tris, pH 7.4), the carbenoxolone (CBX) concentration was adjusted, and the vesicles were incubated for minimum 1 h at room temperature. After monitoring a stable base line for ~30 s, 10 μl of 30 mM sodium ascorbate in buffer was added, and the absorbance was followed for 6 min. The total amount of entrapped cytochrome *c* in both vesicle suspensions (Panx proteoliposomes and control vesicles without pannexons) was determined by rupturing the vesicles with Triton X-100 and set to 100%. The control curves were subtracted from those obtained with the Panx proteoliposomes to extract the pannexon-mediated reduction of cytochrome *c*. To plot the concentration-dependent blocking of the pannexon channels, the initial slopes were determined, normalized, and plotted *versus* the CBX concentration.

Electrophysiology of Xenopus Oocytes—Preparation of Panx1 mRNA, oocytes, and electrophysiological recordings were performed as previously described (15, 37). Pannexin2, in pRK5, was linearized with HpaI. *In vitro* transcription was performed with the polymerases SP6, using the Message Machine kit (Ambion, Austin, TX). mRNAs were quantified by absorbance (260 nm), and the proportion of full-length transcripts was checked by agarose gel electrophoresis. *In vitro* transcribed mRNAs (~20 nl) were injected into *Xenopus* oocytes. For measurement of membrane currents, oocytes expressing pannexins were held at −60 mV, and pulses to −60 mV were applied to transiently open the channels. A 70-s −100 to +100 mV ramp was also applied to Panx2-expressing oocytes. Inhibitor concentrations used were 10 and 100 μM CBX and 1 mM Probenecid. Cytoplasmic acidification experiments using CO_2 were performed as described in Ref. 38.

RESULTS

Membrane topology studies, hydrophobicity plots, and secondary structure predictions revealed that these proteins have several similarities to connexins (four transmembrane segments, the C and N termini facing the cytoplasm, and two extracellular loops containing conserved disulfide bonds) (3, 4, 12, 15, 17). Based on this, pannexins should form connexon-like or gap junction channel-like structures, and early functional studies demonstrated that pannexons might perform a similar function as connexons (11, 21).

Pannexin1 and Pannexin2 Show Connexin-like Channels in Isolated Membrane Preparation—We wanted to study the features of Panx1 and Panx2 channels in native mammalian membranes. To see whether there is any structural homology between pannexin and connexin channels inside of mammalian cell membranes, MDCK cells stably expressing Panx1 or Panx2 were made. Following procedures used in our laboratory for connexin membrane purification by detergent solubilization and sucrose gradient cellular fractionation methods, Panxs membranes were isolated, negatively stained with uranyl acetate, and imaged by EM.

Under conventional imaging methods, our EM analysis showed an overall similarity between the channels formed by

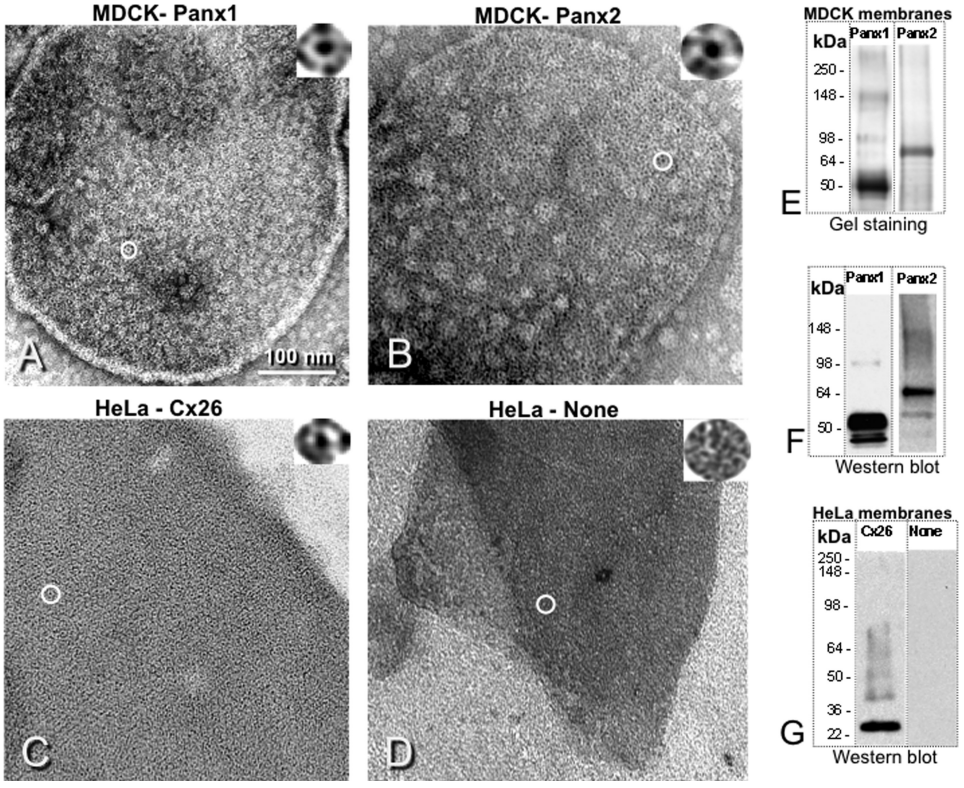

FIGURE 1. **Panx1 and Panx2 show a channel topology in mammalian cell membrane, very similar to gap junction proteins.** Membranes isolated from Panx1 (*A*) and Panx2 (*B*) exogenously overexpressed in MDCK cells contain channel-like structures similar in appearance to Cx26 exogenously expressed in HeLa cells (*C*). As a negative control, a membrane isolated from parental HeLa cells shows no channel-like structures (*D*). Gel staining (*E*) and Western blot (*F*) on denaturing PAGE gels show good purity and high specificity of our membrane purifications. A positive control shows a Cx26 band (*G*) but after stripping and reprobing the same filter with several other antibodies shows no cross-reactivity. The antibodies used in this figure are monoclonal Cx26, our monoclonal Panx1, and polyclonal Panx2 antibodies described under "Experimental Procedures."

Panx1 or Panx2 in MDCK membranes (Fig. 1, *A* and *B*, respectively) and the ones showed by Cx26 in HeLa cells (Fig. 1*C*). As a negative control, membranes isolated from parental HeLa cells, deficient in connexin or pannexin expression, did not reveal any channel-like structures. These membrane preparations were of good purity as confirmed by stained protein gels and Western blots, confirming that the channels visible by EM in the membranes are actually formed by Panx1 or Panx2 proteins (Fig. 1, *E* and *F*).

Although it is possible that channels visible in the membranes isolated from MDCK cells stably expressing Panx2 may be due to the induction of Cx43 found endogenously expressed in some MDCK lines (39), the Western blot filter containing Panx2 was stripped and rehybridized with an antibody against Cx43. As expected only a very low signal was detected after overnight exposure of the filter indicative of either no or very minimal expression of Cx43. Thus, the channels we saw in the EM images are formed by Panx2 oligomers, and this was confirmed by immunogold labeling the membranes on the grid. The membranes showing Panx1 or Panx2 channels were adsorbed on carbon-coated grids for 1 min. The membrane-mounted grids were then dipped in a 50-μl drop of blocking solution (BSA-Tris buffer and 5% goat serum) for 30 min. After blocking, the grids were washed by dipping them for few seconds in drops of BSA-Tris buffer (see "Experimental Procedures"). Incubation with Panx1 or Panx2 primary antibodies in BSA-Tris buffer with 1% of goat serum was made for 1 h at room temperature. The grids were washed again as above and incubated with gold-conjugated secondary antibodies for 1 h at room temperature. After the immunogold process, the grids were washed with double distilled water and negatively stained with uranyl acetate. The EM analysis showed Panx1 or Panx2 membranes covered by black spheres of gold beads, surrounded by gray areas with no or very few gold beads, confirming that the antibodies specifically recognized the channels present on the membranes. The membranes isolated from Cx26 expressing and parental HeLa cells were used for positive and negative controls, respectively, for EM (Fig. 1, *C* and *D*) and Western blot (Fig. 1*G*). In these Western blots, a clear band for Cx26 is visible in the positive control, whereas no bands appeared on the negative control after hybridization with anti-Cx26, anti-Panx1, or anti-Panx2 antibodies.

Membrane Cross-sections Highlight Different Features between Panx1 or Panx2 Membranes and Cx26 Gap Junctions—Fig. 2 contains thin sections through Panx1 and Panx2 membrane pellets that confirmed that we isolated channels in single membranes. These images were in contrast to Cx26 gap junction cross-sections having the classical double plasma membrane and channel striations typical for gap junctions. These data confirmed previous studies, including the one from our group, where Panx1 in mammalian cells was found to form only single membrane assemblies (3, 15, 17, 40). Thin sections performed on immunogold labeled membranes often appeared circular (Fig. 2*B*) with gold spheres *only* on the one external side presumed to be the cytoplasmic surface because the primary antibodies were against cytoplasmic domain peptides. Immunogold secondary antibodies against primary antibodies targeted to a cytoplasmic epitope of Cx26 specifically attached to both sides. Higher magnifications of these membranes showing additional details are shown in Fig. 2*C*.

Purification of Pannexin1 and Pannexin2 Oligomers (Pannexons) in Insect Cells Provides an EM Comparison with Connexons—We purified Panx1, Panx2, and four connexins (Cx26, Cx43, Cx46, and Cx50) from Sf9 insect cells infected with baculoviruses expressing each protein. Cx26 was chosen because it is the second smallest connexin, and the 3D structure has been solved to a resolution better than 10 Å by EM (31) and 3.5 Å by x-ray crystallographic methods (41). We also compared Cx43, the best studied connexin. Cx46 and Cx50 were chosen because they have similar molecular masses. Fig. 3*A*

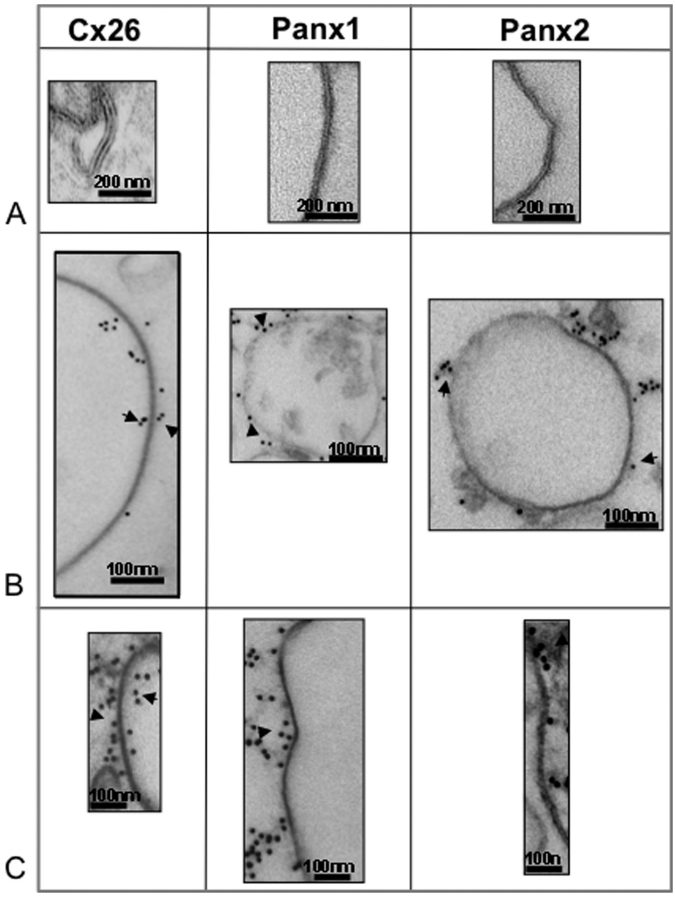

FIGURE 2. **Membrane cross-section comparison between Cx26 and Panx1 or Panx2 showing relevant differences.** Membrane profiles of Cx26, Panx1, and Panx2 show double layers for Cx26 and single layer for Panx1 and Panx2 (*A*). Immunolabeling with specific primary antibodies and with secondary gold conjugated antibodies shows that the gold labels both sides of the membrane profile for Cx26 and only one side for Panx1 and Panx2 (*B*). An enlarged view of an immunolabeled membrane is shown (*C*) for easier visualization.

contains images of purified oligomers of Cx26 (*top left panel*) to Panx2 (*bottom right panel*). The oligomers appear larger in a correspondence with the increasing monomer molecular mass. Cx26 oligomers tend to have a uniform appearance indicative of few orientations on the grid and display small doughnut-like structures with a clear pore. Oligomers of larger connexins or pannexins have a more heterogeneous appearance, perhaps indicating different orientations on the carbon-coated grids. For Cx50 and Panx2 oligomers, it is clear that we have at least two different morphologies that we would attribute to two different orientations of the channels in combination with differential staining (*black* and *white circled oligomers* with *black* and *white boxed insets,* respectively). To confirm the nature of our protein preparations and to check their purity, we performed gel staining and Western blots after electrophoresis in denaturing conditions (Fig. 3*B*). As expected, the molecular masses of these proteins increase from Cx26 (*left lanes*) to Panx2 (*right lanes*). Comparing stained protein gels (*left lanes* labeled with G for gel) and the Western blot (*right lanes* labeled with W for Western blot) for the same sample of each protein analyzed, we see a good correspondence of bands; however, dimeric bands are more intense in the Western blots because of the inherent nature of this enzymatic reaction enhancing the signal intensity. Thus, these samples contain homogeneous populations of connexons or pannexons.

Size Analysis of Pannexons and Connexons after Two-dimensional Image Averaging—We next compared connexons and pannexons for their oligomeric size and pore diameters. Because these assemblies are small compared with most single-particle reconstruction specimens, following a published method (42), we used negative staining in combination with cross-linking of the oligomers prior to imaging to maintain a stable structure. Particles were imaged and boxed for two-dimensional reconstruction. At this resolution (low dose and 40,000 magnification), averaged images, of views with a clear pore, showed similarities between connexons (30 particles averaged) and pannexons (50 particles averaged) (supplemental Fig. S1). We applied circular symmetry to these averaged images to get more accurate measurement of sizes and diameters of the particles. For Panx1 and Panx2 in these conditions, we saw different morphologies of pannexons and the larger connexons (*e.g.* Cx50) within these images indicative of different orientations of the particle on the grid. Although the pore diameters of the different isoforms of pannexons were similar, the oligomer diameters increased in correspondence with the protein molecular mass. Supplemental Fig. S1 (*middle column*) contains two image averages of pannexons with different diameters (oligomer diameters ~120 and 160 Å for Panx1 and oligomer diameters ~183 and 190 Å for Panx2). On the other hand, Cx26, the smallest of the connexins we examined, tended to have a small number of unique orientations on the grid (oligomer diameter, ~81 Å). In projection, the measured pore diameter for Cx26 is substantially smaller (~12.5 Å) than for Panx1 (~21 and 17 Å) or Panx2 (~29.5 and 30.5 Å).

Purified Panx1 and Panx2 Pannexons Form Open Channels—To test whether these pannexons were functional, Panx1 and Panx2 baculovirus Sf9 pannexon preparations were used in a cytochrome *c* liposome-based assay used in several previous studies (33–36) (Fig. 4). Briefly, cytochrome *c* was trapped insight a 200-nm-diameter proteoliposome. After the addition of ascorbate and in the presence of open channels through which ascorbate can pass but not cytochrome *c*, cytochrome *c* was reduced (Fig. 4*A*). Using a Sephadex G-75 column, free cytochrome *c* can effectively be separated from Panx proteoliposomes with entrapped cytochrome *c* (Fig. 4*B*). The reduction of cytochrome *c* was measured at 417 nm using an UV-visible spectrophotometer. For these vesicle assays, we did the negative control measurements of liposomes without protein to quantify the background signal. We measured the vesicles with protein and CBX. Then we measured the control vesicles without protein, but in the presence of CBX. The control curves were subtracted from the curves gained with protein. As a positive control for this assay, we used a different protein/oligomer. Cx26 connexons inserted into liposomes containing entrapped cytochrome *c* were inhibited by CBX, α-cyclodextrin, and calcium ions in good agreement with the literature data. For both Panx1 and Panx2 proteoliposomes, we saw a time-dependent significant reduction of intraliposomal cytochrome *c* (Fig. 4, *C* and *D*, *top line*). CBX was added at different concentrations to analyze whether it is able to block the reconstituted pannexons. Although the reduction of cytochrome *c* itself was not influ-

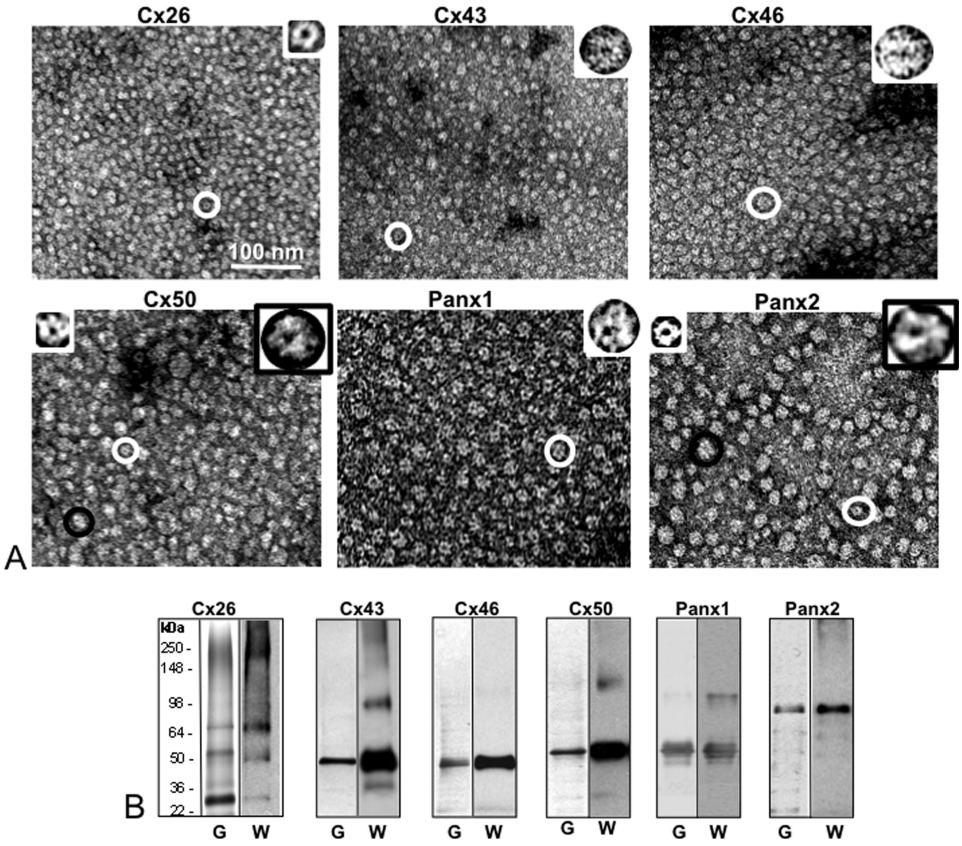

FIGURE 3. **Isolated pannexin oligomers (pannexons) confirm similar features to connexons.** Pannexons and connexons expressed and purified from baculovirus infected Sf9 cells. *A*, EM analysis going from a smaller connexin (Cx26 *top left image*) to Panx2 (*bottom right image*). Larger proteins (Panx2 and Cx50) have more heterogeneous morphology of structures, perhaps because of differential staining of different orientations. The images are displayed at the same magnification to show increasing channel size with increasing monomer size. *B*, stained protein gels (labeled with *G* for gel on the bottom) and Western blots (labeled with *W* for Western blot) by the side of each protein demonstrate good purity of these preparations. Note that Western blots can tend to overemphasize dimeric bands. *White circles* and *white boxed insets* indicate oligomers that have smaller diameters than ones with *black circles* and in *black box insets*.

enced by CBX, the treatment of reconstituted Panx1 pannexons with CBX resulted in a concentration-dependent decrease in channel activity with an $IC_{50} = 14 \pm 4$ μM being similar to published results (21) (Fig. 4, *C* and *E*). Similarly, Panx2 channels were incorporated into proteoliposomes, and their activity was inhibited by CBX with an $IC_{50} = 15 \pm 4$ μM (Fig. 4, *D* and *F*). Thus, this is the first report of functional Panx2 homomeric pannexons, because the assay does not depend on the channels being expressed on the plasma membrane.

Panx1 and Panx2 Homomeric Channels Have a Different Physiological Profile from Each Other When Expressed in Single Xenopus Oocytes—Panx2 has previously been reported to be nonfunctional in *Xenopus* oocytes except when in combination with Panx1 (11, 21). However, it should be noted that the rat Panx2 construct we used in this study was 10 amino acids longer at the beginning of the N terminus (22) than the one used in Ref. 11. This longer protein is found in healthy and ischemic brains of adult rats (22). It is not known whether the shorter Panx2 pannexon is found in tissue. However, we did not find any differences in structure or trafficking in similar experiments that used the shorter construct. Because we found activity in an *in vitro* permeability assay, we repeated expression of Panx2 in single *Xenopus* oocytes. Although we found that Panx1 channels opened in response to extracellular K^+ even at negative holding potentials (10), Panx2 channels did not. To test for voltage-dependent opening of the channels, we applied voltage ramps to transiently open them. Panx2 channels only opened when a slow (70 s) −100 mV to +100 mV ramp was applied and 2.14 ± 0.13 μA ($n = 6$) current was recorded (Fig. 5*A* and Table 1), and these currents were unaffected by high concentrations of CBX (100 μM; Fig. 5*B*) or Probenecid (1 mM; supplemental Fig. S2). The large currents in Panx2-expressing oocytes were detected in 21 of 21 cells from four ovaries with little variation in amplitude (Table 2). Uninjected oocytes exhibited significantly smaller currents. We also found that when Panx1 and Panx2 were co-expressed in *Xenopus* oocytes in a 1:1 ratio, there was a reduction in current from 1.96 ± 0.31 μA ($n = 6$) to 0.86 ± 0.31 μA ($n = 6$) (Table 1), indicating a mutual inhibition between the two pannexins. This result is in agreement with measurements of dye uptake in Panx1 and Panx2 exogenously co-expressing HEK293T cells made by Penuela *et al.* (20).

To test whether these currents were due solely to the opening of Panx2 channels, we constructed four cysteine mutants. Panx2 has four conserved cysteines, two in each of the extracellular loops, as do all members of the pannexin/innexin superfamily. These four cysteines are Cys^{81}, Cys^{99}, Cys^{259}, and Cys^{280}. They may serve a similar function in disulfide bonding as the six cysteines in connexins. As we found previously for connexins and Panx1, mutation of any of these extracellular cysteines in Panx2 resulted in a loss of function (Fig. 5*C* and Table 1), indicating that the currents observed with WT Panx2 channels are attributable to this protein and do not represent endogenous currents activated by the Panx2 expression. These Panx2-specific currents are also supported by the observation that Panx2 WT-expressing oocytes were sensitive to cytoplasmic acidification as are all gap junction proteins (supplemental Fig. S3 and Table 3). Perfusion of uninjected oocytes triggered the appearance of large membrane currents at positive potentials, which were not significantly enhanced in Panx2-expressing oocytes, indicating closure of Panx2 channels by cytoplasmic acidification (Table 3).

Panx2 Does Not Form Hexamers—Although we have previously established that Panx1 forms hexamers, we investigated whether a similar symmetry exists in Panx2 oligomers. Panx2-V5-His was expressed and purified using the baculovirus Sf9 expression system. After purification we analyzed Panx2 oligo-

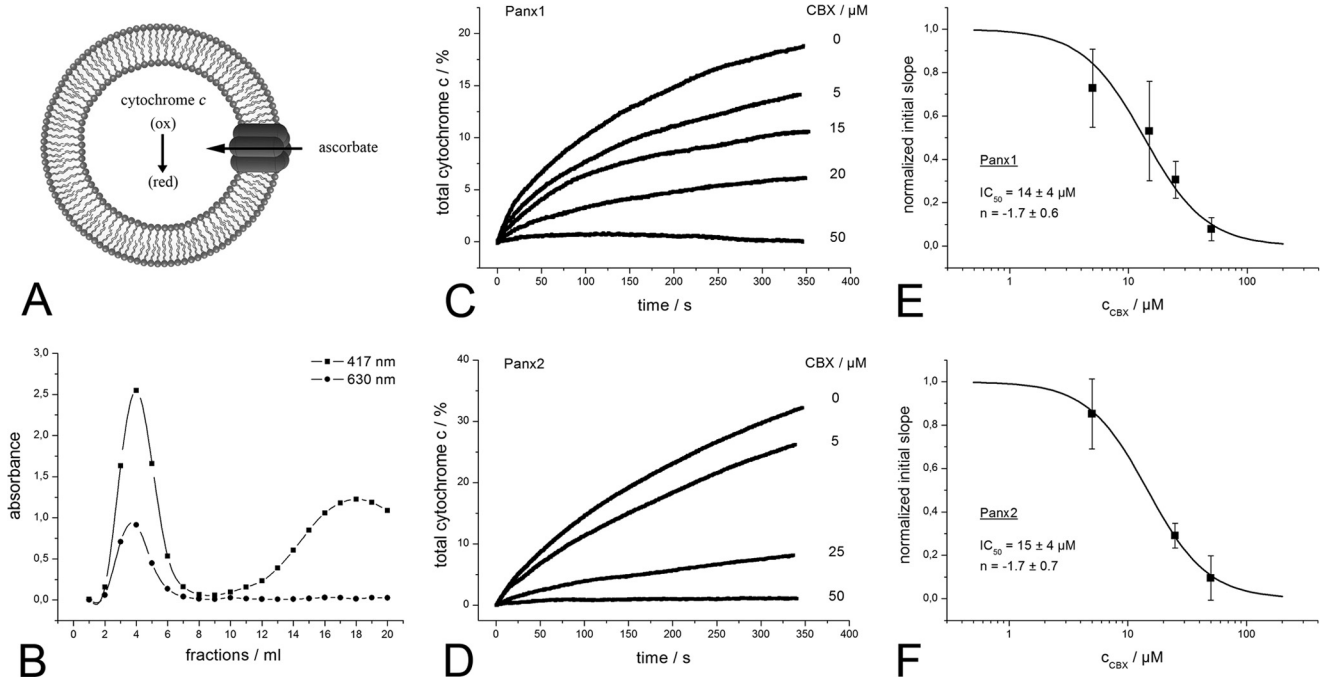

FIGURE 4. **Panx2 homomeric channels are functional.** *A*, schematic of the cytochrome *c*-based vesicle assay. If Panx2 channels are functionally reconstituted, ascorbate crosses the lipid bilayer. Intraliposomal cytochrome *c* gets reduced as monitored at 417 nm. *B*, fractions of a characteristic size exclusion chromatography to separate free cytochrome *c* from Panx-1-palmitoyl-2-oleoyl-*sn*-glycero-3-phosphocholine-proteoliposomes with entrapped cytochrome *c*. Turbidity of the vesicle suspension is followed at 630-nm, cytochrome *c*-containing fractions at 417 nm. *C*, time-resolved reduction of intraliposomal cytochrome *c* mediated by the transport of ascorbate via a transmembrane spanning active Panx1 channel and inhibition with CBX. *D*, as in *C* for Panx2. *E*, semi-logarithmic plot illustrating the concentration-dependent blocking of the Panx1 pannexons by CBX. Each data point represents the normalized initial slope m_i of the Panx1-mediated intraliposomal cytochrome *c* reduction. The *solid line* is a fit to the data points using the Hill equation of the form: $m_i = m_{i\,MAX}\,(c_{CBX}{}^{-n}/([IC_{50}]^{-n} + c_{CBX}{}^{-n}))$ where $m_{i\,MAX}$ is the initial slope recorded in buffer without CBX (set as unity), c_{CBX} is the drug concentration, IC_{50} is the concentration giving half of the maximal inhibition, and *n* is the Hill coefficient. *F*, as in *E* for Panx2.

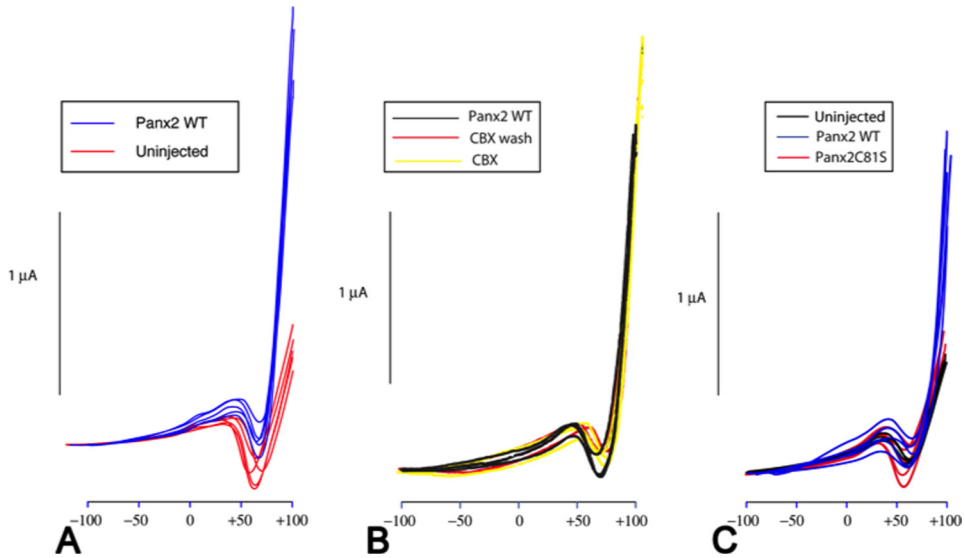

FIGURE 5. **Panx2 channels expressed in *Xenopus* oocytes opened at high positive membrane potentials and were insensitive to inhibitors.** A voltage ramp from −100 mV to +100 mV over a span of 70 s applied to single, uninjected oocytes induced a transient inward current carried by endogenous channels (probably voltage activated sodium channels) (*red traces* in *A*). These currents were somewhat variable between oocytes and even within the same oocyte in response to repetitive activation as indicated by the variability of the amplitude and position of peak activity. Expression of Panx2 resulted in large outward currents most prominent at potentials exceeding +75 mV (*blue traces*). Shown here are five representative traces from each condition. Membrane currents in Panx2-expressing oocytes before (*black traces*), during (*yellow traces*), and after washout (*red traces*) of CBX are shown in *B*. CBX slightly attenuated the endogenous inward currents and led to larger peak currents as if stimulating rather than inhibiting Panx2 currents, an effect that was not immediately reversed upon washout. This figure contains three traces each for Panx2 WT-injected oocytes and subsequent CBX-treated oocytes and two traces for the CBX wash out oocytes. In *C*, mutagenesis of cysteines in Panx2 eliminated currents in injected oocytes (see also Table 2). Shown here are five representative traces from the Panx2C81S mutant, Panx2 WT, and uninjected oocytes.

meric state by cross-linking with DSP 300 μg/ml following a protocol similar to the one applied to study Panx1 oligomers (15). Because of the larger size of Panx2 (~70 kDa) *versus* Panx1 (~48 kDa), we found that our original gel analysis system was not accurate enough to definitely distinguish between hexamers, heptamers, or octamers. In Fig. 6*B* we show the Western blot of Panx2 cross-linked on 4% Tris-glycine gel PAGE. The cross-linked Panx2 band mapped well above the position of the high molecular mass marker at 500 kDa. Thus, Panx2 does not form a hexamer that would be expected below the 500-kDa marker band (~70 kDa × 6 = 420 kDa).

To better resolve the Panx2 oligomeric state, we constructed a truncated version of Panx2 sequence. Secondary structure prediction algorithms run on the C terminus of Panx2 contained some predicted α-helices and β-strands separated by extended areas of random coil. A truncation site between Ser^{340} and

Gln^{341} was chosen because it was close to the membrane (Figs. 6, *A* and *C*) just after the first predicted helical segment and intermediate to the next secondary structure element (Fig. 6*D*). This truncation mutant contained the first 340 amino acids (Panx2Trun340) plus a 30-amino acid V5-His_6 tag for a predicted molecular mass of ~40.7 kDa. This molecular mass of Panx2Trun340 was somewhat smaller than Panx1 (~48 kDa). When Panx2Trun340-Myc was expressed in HEK293 tissue culture cells, we found it had similar expression and trafficking to the full-length Panx2-Myc.

A baculovirus containing Panx2Trun340-V5-His_6 was generated and expressed in Sf9 cells. Channel structures were purified and analyzed with two different gel systems as we had previously done in our initial Panx1 studies (15). In Fig. 6, we show two diagrams comparing the sequences of full-length and Panx2Trun340 (Fig. 6, *A* and *C*) and the molecular mass of the monomer on denaturing gel (Fig. 6*E*). Cytochrome *c* vesicle assays as performed in Fig. 4 showed that truncated Panx2 pannexons inserted into liposomes were less permeable to ascorbate and full-length Panx1 and Panx2 (Fig. 6*F*). Because we observed that truncated Panx2 is still able to oligomerize and form channels by EM (Fig. 6*G*), we performed cross-linking as described above for full-length Panx2. On Tris-glycine gel 4–20%, the highest band mapped above the 250 kDa of the marker, confirming that the oligomer cannot be a hexamer, which in this case was supposed to map ~246 kDa (41 kDa × 6 = 246 kDa). The cross-linked sample boiled in the presence of 5% β-mercaptoethanol (a condition that breaks the cross-linked bonds) showed the monomeric band as expected, mapping ~41 kDa (Fig. 6*H*). To confirm our result and better resolve our bands, we used a Tris-acetate 3–8% gel (Fig. 6*I*) with the high molecular mass marker that clearly showed the monomer corresponding to 41 kDa, the dimer corresponding to ~82 kDa, and the upper band between above the 268 kDa but lower than the 460-kDa marker band. This evidence confirms that the oligomeric state of Panx2 is not a hexamer but rather a heptamer or octamer. When purified cross-linked Panx1-V5-His_6 oligomers were run in side-by-side experiments with Panx2Trun340-V5-His_6 oligomers (Fig. 6*J*), the mobility of the hexameric band of Panx1 was higher than the truncated Panx2. Estimation of molecular masses indicates that the Panx1-V5-His_6 band matches the expected calculated hexameric mass (~288 kDa), whereas the center of the Panx2Trun340-V5-His_6 band (~326 kDa) can only be explained by an octameric oligomerization number (8 × 41 kDa = 328 kDa). The calculated 287-kDa molecular mass for a heptameric Panx2Trun340-V5-His_6 channel would be approximately the same molecular mass as Panx1-V5-His_6 hexamers (288 kDa); however, the data in Fig. 6*J* show a clear separation. Thus, these data clearly indicate that Panx2 is an octamer. In our EM analysis, we found that Panx2Trun340-V5-His_6 channels (Fig. 6*G*) were more labile than cross-linked Panx2Trun340-V5-His_6 channels (Fig. 6*K*), suggesting that the negative staining process can affect Panx2Trun340-V5-His_6 stability. However, in each micrograph, many discrete channel structures are identifiable. Thus, these results indicate that the Panx2 channel does not have hexameric symmetry, but rather, it is most probably an octamer because this oligomer number matched better with the experimental data.

Panx1 and Panx2 Form Unstable Heteromeric Channels—Given the symmetry mismatch between Panx1 and Panx2 homomeric pannexons, we wondered how Panx1 and Panx2 could mix together in forming heteromeric channels described before by other authors (11, 20). To isolate Panx1/Panx2 heteromeric channels in insect cells, we co-expressed Panx1-V5-His_6 tag and full-length Panx2-no tag baculoviruses in ratios of 1:1, 1:2, or 1:4. Using this strategy as we have previously published (23), only homomeric Panx1 or heteromeric Panx1/Panx2 would be isolated, whereas we did not expect any homomeric channels for Panx2, given the lack of the His tag for this construct. The only way Panx2-no tag could be isolated after co-infection in insect cells with Panx1-V5-His_6 would be if it formed heteromers with Panx1-V5-His_6. After purification, the Western blot on these samples showed both the presence of Panx1 and Panx2 (Fig. 7*C*), suggesting that they co-purified. EM images of the same samples taken one or a few hours after the purification showed a more heterogeneous looking preparation than Panx1 or Panx2 purified singularly but contained "doughnut" like appearances (Fig. 7*A*), suggesting that we have Panx2

TABLE 1

Co-expression of Panx1 and Panx2 in Xenopus oocytes

The mRNAs for Panx1 and Panx2 were mixed with each other or with water at equal volumes to have identical concentrations for each experimental condition. The currents at +100 mV at the end of a voltage ramp from −100 to +100 mV were analyzed.

	Panx1	Panx2	Panx1 + Panx2	Uninjected
Mean current (mA)	1.96	2.14	0.86	0.44
S.E.	0.31	0.13	0.17	0.02
n	6	6	6	4

TABLE 2

Mutagenesis of extracellular cysteines causes elimination of currents in Xenopus oocytes

The mRNAs for Panx2 and four cysteine to serine substitution mutants were injected into oocytes, and voltage ramps were applied as previously described. Maximal current amplitudes at the end of voltage ramps (+100 mV) were analyzed and plotted.

	Uninjected	Panx2	C81S	C99S	C259S	C280S
Mean (μA)	0.54	1.78	0.71	0.68	0.58	0.62
S.E.	0.02	0.10	0.03	0.02	0.01	0.01
n	20	21	5	5	5	5

TABLE 3

Effect of CO_2 on Panx2 channel currents

The oocytes were treated with CO_2 that induces cytoplasmic acidification. The subscript "CO2" refers to oocytes treated with CO_2. Panx2 channel-specific currents were assessed by subtracting currents measured in uninjected oocytes from currents in Panx2 injected oocytes without (second to right-hand column) and with (right-hand column) CO2 perfusion.

	Uninjected	$Uninjected_{CO2}$	Panx2	$Panx2_{CO2}$	Panx2-Uninjected	$Panx2_{CO2}$-$Uninjected_{CO2}$
Mean (μA)	0.46	1.56	1.14	1.66	0.68	0.1
S.E.	0.02	0.12	0.05	0.08		
n	5	5	5	5		

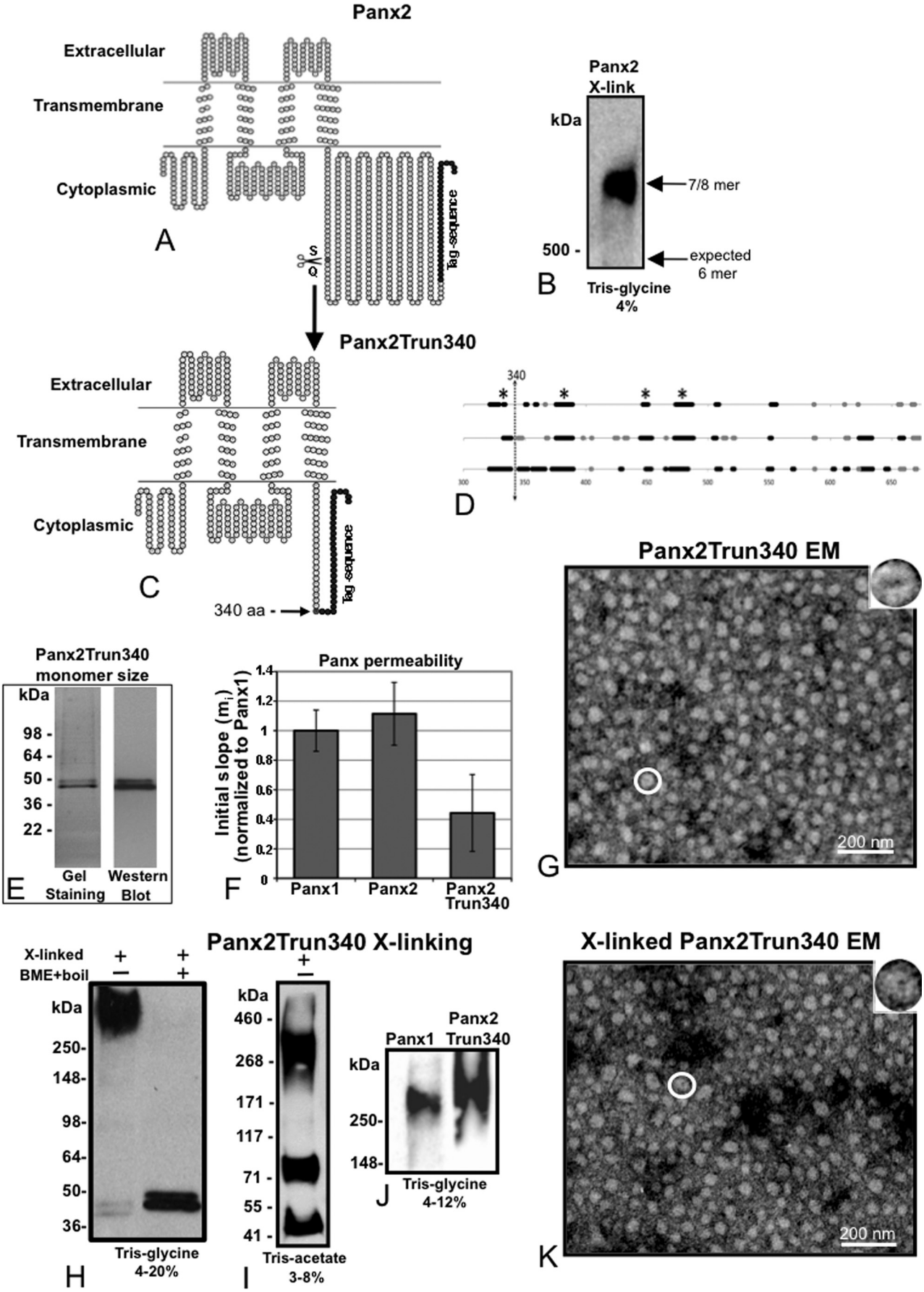
Panx2
Extracellular
Transmembrane
Cytoplasmic
epitope-tag
A
Panx2
X-link
kDa
7/8 mer
500 -
expected
6 mer
B
Tris-glycine
4%
Panx2Trun340
Extracellular
Transmembrane
Cytoplasmic
epitope-tag
340 aa -
C
340
D
Panx2Trun340 EM
200 nm
G
Panx2Trun340
monomer size
kDa
98 -
64 -
50 -
36 -
22 -
Gel
Staining
Western
Blot
E
Panx permeability
Initial slope (m_i)
(normalized to Panx1)
1.4
1.2
1
0.8
0.6
0.4
0.2
0
Panx1
Panx2
Panx2
Trun340
F
Panx2Trun340 X-linking
X-linked
BME+boil
kDa
250-
148-
98-
64-
50-
36-
Tris-glycine
4-20%
H
kDa
460 -
268 -
171 -
117 -
71 -
55 -
41 -
Tris-acetate
3-8%
I
Panx1
Panx2
Trun340
kDa
250-
148-
Tris-glycine
4-12%
J
X-linked Panx2Trun340 EM
200 nm
K

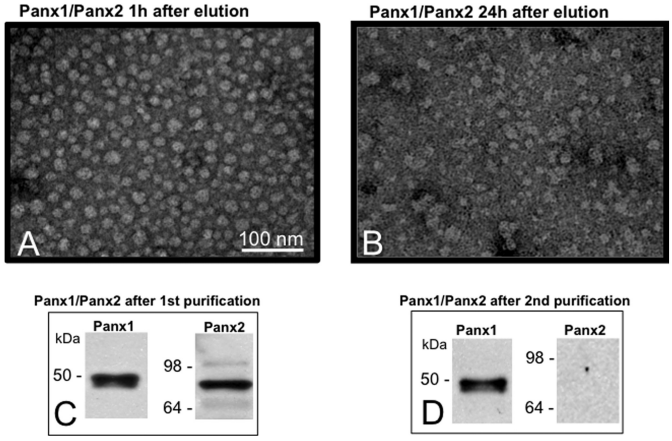

FIGURE 7. **Panx1/Panx2 heteromers are highly unstable.** *A*, EM image containing negatively stained Panx1/Panx2 oligomers examined 1 h after purification. *B*, after 24 h, the channels are barely recognizable. *C*, the 1-h sample analyzed by Western blot contained both Panx1 and Panx2 bands. *D*, after buffer exchange and a second nickel-nitrilotriacetic acid affinity column purification, Panx1 bands are evident, but not Panx2.

integrated in heteromeric channels together with Panx1, probably mixed to Panx1 homomeric channels as well. Twenty-four hours after the purification, the sample was highly heterogeneous without the appearance of channel structures (Fig. 7*B*), revealing high instability for these channels. To understand whether the high instability would be caused by disaggregation of Panx1-V5-His_6 and Panx2, we used a second resin purification step for the sample after 24 h. Using a buffer exchange column, we replaced the elution buffer containing high concentration of L-histidine with a binding buffer (lacking L-histidine). We incubated our sample a second time with new nickel-nitrilotriacetic acid-nickel resin overnight. After elution with L-histidine, Western blots showed Panx1 bands at ~50 kDa (unglycosylated and glycosylated), whereas the filters hybridized with anti-Panx2 antibody contained no Panx2 bands (Fig. 7*D*). These data demonstrate that Panx1 and Panx2 can form heteromeric channels, but they are very unstable and disaggregate within few hours. Thus, this helps to explain why Panx1 and Panx2 can form heteromers in some expression systems such as *Xenopus* oocytes (11) and HEK293 cells (20), but our group and others (43) see a clear separation of homomeric Panx1 and Panx2 channels in stably expressed mammalian cells and brain tissue.[3]

DISCUSSION

Pannexin channels represent a novel channel assembly with functions distinct from connexin channels or connexons but sharing some structural features. Published studies have concentrated on their trafficking, expression, and function in mammalian cells and tissues, whereas this work is focused on their structural characterization at the molecular level.

Pannexin Structures Isolated from Mammalian and Insect Cells—We showed for the first time that when exogenously expressed in mammalian cells, Panx1 and Panx2 oligomers in isolated membranes look very similar to connexin gap junction channels. Despite this structural homology between connexons and pannexons, our group and others have shown that Panxs do not form gap junctions (3, 15, 17). For Panx1 and Panx3, a carbohydrate tree at a unique Asn in the extracellular loops would sterically hinder gap junction formation (3, 15, 44). Panx2 also contains a unique glycosylation site (20) that may prevent docking; however, it is unclear whether this isoform is fully glycosylated in native systems (43). In this study, we reconfirmed again using Panx1 and Panx2 membrane isolations that cross-sections through pelleted membrane preparations contain a single membrane layer with immunogold labels attached to only one side of the membrane in contrast to Cx26 preparations where we find double layers (gap junctions) and immunogold labels attached to both sides.

Pannexons purified from Panx baculovirus-infected insect cell membranes confirmed an overall structural homology between pannexons and connexons, both showing doughnut-like structures across a size range of connexins. Single-particle two-dimensional averages of selected Cx26 connexon and Panx1 or Panx2 pannexon images were compared for their size and pore diameter. The measurements revealed an increasing oligomer diameter commensurate with an increase in the monomer molecular mass. As the particle size increased, the images appeared more heterogeneous because of different orientations on the grid. Pore diameters for Panx1 and Panx2 were larger than for Cx26, and Panx1 pore diameters were smaller than Panx2. However, it should be emphasized that diameters were measured from two-dimensional averaged projection images, and the expectation is that the pore has different diameters along its axis perpendicular to the membrane plane. The monomer molecular mass of Panx2 is ~45% larger than Panx1 with

FIGURE 6. **Cross-linking of a Panx2 truncation mutant for stoichiometric analysis reveal nonhexameric assemblies.** *A*, folding diagrams for full-length Panx2. *B*, cross-linked Panx2 run on a 4% Tris-glycine gel reveals a band located well above a hexamer. This band corresponds to either a heptamer or octamer. To distinguish between an octamer and heptamer stoichiometry, a truncation mutant of Panx2 was constructed so that Panx2 is truncated after Ser^{340} plus a 30-amino acid tag (370 amino acids total). *C*, topology diagram for Panx2Trun340-V5-His_6. *D*, predicted secondary structure in the Panx2 C terminus (amino acids 317–674) according to three different prediction algorithms NNPredict (*top*), GOR4 (*middle*), and PSIPRED (*bottom*). *Heavy black lines* mark stretches of putative α-helices, and *heavy gray lines* indicate β structure propensity. An *asterisk* denotes predicted secondary structure elements longer than 3 amino acids common among these three predictions. The *dotted arrow* indicates the truncation position between Ser^{340} and Gln^{341}. *E*, purified Panx2Trun340-V5-His_6 preparations were analyzed by gel stainings and Western blots that this protein maps at ~41 kDa as expected. Truncated Panx2 was cross-linked with DSP 300 μg/ml after purification and analyzed on different gels. *F*, cytochrome *c* vesicle permeability measurements comparing Panx1-V5-His_6, Panx2 WT V5-His_6, and Panx2Trun340 V5-His_6 (as in Fig. 4). Comparison of the initial slopes m_i of the fitted line to data points recorded during the first 25 s after the addition of ascorbate for the three pannexons indicated that Panx2 truncation pannexons had a reduced permeability to ascorbate. Each category has an $n = 3$. *G*, electron micrograph shows channels formed by Panx2Trun340-V5-His_6. *H*, *left lane*, Panx2 shows the upper band mapping above 250 kDa, suggesting that it is not a hexamer (41 kDa × 6 = 246 kDa). *Right lane*, cross-linked Panx2 was boiled in the presence of 5% β-mercaptoethanol and shows the monomeric band mapping as expected ~41 kDa. *I*, cross-linked Panx2Trun340-V5-His_6 is run on a higher resolving Tris-acetate gel system and is separated into the monomer (41 kDa), the dimer (82 kDa), and the upper band mapping between 268 and 460 kDa. *J*, the cross-linked Panx2Trun340-V5-His_6 upper band maps higher than Panx1 hexameric band (~300 kDa). The measured position of the Panx2Trun340-V5-His_6 band is at a position that confirms that the Panx2 oligomer is mostly likely an octamer. *K*, electron micrograph shows Panx2Trun340-V5-His_6 channel appearance after cross-linking. All baculovirus/purified proteins have a C-terminal V5-His_6 tag.

the major addition of mass predicted to be in the C terminus (~128 amino acids for Panx1 C terminus *versus* ~366 amino acids for Panx2 C terminus). In addition, the N terminus domain of Panx2 is also larger, containing 52 amino acids *versus* 36 amino acids for Panx1 and 21 residues for Cx43. Surprisingly, cross-linking studies to determine stoichiometry using full-length and a Panx2 truncation mutant revealed the oligomeric state of this protein not being a hexamer as Panx1 (15) but fits the data best as an octamer. Given the conserved hexameric state of all connexons and of Panx1 pannexons and the conservation of folding of connexins and pannexins, this was unexpected. However, it is possible that to make a closed structure to accommodate the larger monomer size of Panx2 (and bulky cytoplasmic domains), the oligomer number needs to increase to eight.

Panx2 Channels Are a Unique Functional Entity, Distinct from Panx1—First reports by Bruzzone *et al.* (11) indicated that Panx2 was only expressed at the plasma membrane in combination with Panx1, as was found for co-expression of *Drosophila* Inx2 and Inx3 (45). Data from Lai *et al.* (43) and our lab[3] show a clear separation between Panx1 at the plasma membrane and Panx2 intracellular pools when co-expressed in several cell lines or in high resolution light microscopic localization in tissues. Recently, Penuela *et al.* (20) showed that in HEK293T and NRK cells, Panx2 may form heteromers with Panx1; however, this was based on co-immunopurification of Panx1/Panx2 of whole cell lysates and light level immuno-colocalizations of Panx1 and Panx2 at the plasma membrane. Within the resolution of the light microscope, it is unclear whether in overlapping populations in the plasma membranes, Panx1 and Panx2 make heteromeric channels or form domains of mixed populations of homomeric channels because the plasma membrane contains areas of only Panx1 or Panx2 labeling as well. It is worth noting that we can isolate Panx2 channel-bearing membranes from intracellular compartments, because the isolation protocol we use is not an affinity-based approach but rather selects based on detergent resistance and density gradient fractionation methods. Our functional data from *Xenopus* oocyte studies confirm that Panx2 has an inhibitory effect on Panx1, although it is not known whether this is due to Panx1/Panx2 heteromeric channels being nonfunctional or Panx1 mistrafficking when co-expressed with Panx2.

Here, we show for the first time that Panx2 homomeric channels are functional using a cytochrome *c*-based proteoliposome assay. We also found that Panx2 channels in *Xenopus* oocytes could be opened but only at higher, nonphysiological voltages. These currents were eliminated by mutagenesis of any of the four cysteines in the extracellular loops, indicating that currents in oocytes expressing Panx2 WT could only be attributable to Panx2. In addition, cytoplasmic acidification closed Panx2 channels. The functional studies with the vesicle assay also demonstrated an inhibitor-induced closure of Panx 1 and Panx2 channels. The effect on Panx1 channels is in accordance with previously published studies using single *Xenopus* oocytes (46) (this study). However, in contrast to the vesicle assay, Panx2 channel opening events were not inhibited by CBX or Probenecid in *Xenopus* oocytes. Although this result was surprising, Silverman *et al.* (10) showed that the potassium channel subunit $K_v\beta3$ eliminates inhibitor sensitivity in Panx1 when Panx1 and $K_v\beta3$ are co-expressed. Here the reverse situation is presented, where it is possible that cellular factors not present in the *in vitro* proteoliposome assay can modulate Panx2 to eliminate CBX and Probenecid inhibition. Thus, we propose that Panx2 makes channels that are functionally and structurally different from Panx1 channels. It should also be noted that the elimination of most of the Panx2 C terminus resulted in channels that showed reduced permeability to ascorbate in our vesicle assay system but still made recognizable channel structures.

Finally, we find that when Panx1 and Panx2 are isolated from an overexpression system using an affinity tag for purification, the heteromers can form but are unstable, reflecting the symmetry mismatch between the two isoforms. Taken together with other studies, we speculate that Panx1 and Panx2 do not oligomerize *in vivo* or if they do, their heteromeric associations are unstable or nonfunctional. Although the *in vivo* function of Panx2 channels is still not established, it is clear that Panx2 has unique functional properties and molecular organization that set it apart from Panx1 channels. This structural and functional analysis on purified Panx1 and Panx2 channels lays the foundation for future structure-function studies to understand their unique role in cells and tissues.

Acknowledgments—We thank Norm Olson of the University of California San Diego Cryoelectron Microscopy for guidance and advice. We are also grateful to Mason Mackey for ultramicrotomy.

REFERENCES

1. D'hondt, C., Ponsaerts, R., De Smedt, H., Bultynck, G., and Himpens, B. (2009) *Bioessays* **31,** 953–974
2. Panchin, Y. V. (2005) *J. Exp. Biol.* **208,** 1415–1419
3. Penuela, S., Bhalla, R., Gong, X. Q., Cowan, K. N., Celetti, S. J., Cowan, B. J., Bai, D., Shao, Q., and Laird, D. W. (2007) *J. Cell Sci.* **120,** 3772–3783
4. Baranova, A., Ivanov, D., Petrash, N., Pestova, A., Skoblov, M., Kelmanson, I., Shagin, D., Nazarenko, S., Geraymovych, E., Litvin, O., Tiunova, A., Born, T. L., Usman, N., Staroverov, D., Lukyanov, S., and Panchin, Y. (2004) *Genomics* **83,** 706–716
5. Jiang, H., Zhu, A. G., Mamczur, M., Falck, J. R., Lerea, K. M., and McGiff, J. C. (2007) *Br. J. Pharmacol.* **151,** 1033–1040
6. Dahl, G., and Locovei, S. (2006) *IUBMB Life* **58,** 409–419
7. MacVicar, B. A., and Thompson, R. J. (2010) *Trends Neurosci.* **33,** 93–102
8. Kanneganti, T. D., Lamkanfi, M., Kim, Y. G., Chen, G., Park, J. H., Franchi, L., Vandenabeele, P., and Núñez, G. (2007) *Immunity* **26,** 433–443
9. Pelegrin, P., Barroso-Gutierrez, C., and Surprenant, A. (2008) *J. Immunol.* **180,** 7147–7157
10. Silverman, W. R., de Rivero Vaccari, J. P., Locovei, S., Qiu, F., Carlsson, S. K., Scemes, E., Keane, R. W., and Dahl, G. (2009) *J. Biol. Chem.* **284,** 18143–18151
11. Bruzzone, R., Hormuzdi, S. G., Barbe, M. T., Herb, A., and Monyer, H. (2003) *Proc. Natl. Acad. Sci. U.S.A.* **100,** 13644–13649
12. Panchin, Y., Kelmanson, I., Matz, M., Lukyanov, K., Usman, N., and Lukyanov, S. (2000) *Curr. Biol.* **10,** R473–R474
13. Dahl, G., Werner, R., Levine, E., and Rabadan-Diehl, C. (1992) *Biophys. J.* **62,** 172–182
14. Prochnow, N., Hoffmann, S., Vroman, R., Klooster, J., Bunse, S., Kamermans, M., Dermietzel, R., and Zoidl, G. (2009) *Neuroscience* **162,** 1039–1054
15. Boassa, D., Ambrosi, C., Qiu, F., Dahl, G., Gaietta, G., and Sosinsky, G. (2007) *J. Biol. Chem.* **282,** 31733–31743
16. Verselis, V. K., and Bukauskas, F. F. (2002) *Curr. Drug Targets* **3,** 483–499

17. Locovei, S., Bao, L., and Dahl, G. (2006) *Proc. Natl. Acad. Sci. U.S.A.* **103,** 7655–7659
18. Bao, L., Locovei, S., and Dahl, G. (2004) *FEBS Lett.* **572,** 65–68
19. Huang, Y., Grinspan, J. B., Abrams, C. K., and Scherer, S. S. (2007) *Glia* **55,** 46–56
20. Penuela, S., Bhalla, R., Nag, K., and Laird, D. W. (2009) *Mol. Biol. Cell.* **20,** 4313–4323
21. Bruzzone, R., Barbe, M. T., Jakob, N. J., and Monyer, H. (2005) *J. Neurochem.* **92,** 1033–1043
22. Zappalà, A., Li Volti, G., Serapide, M. F., Pellitteri, R., Falchi, M., La Delia, F., Cicirata, V., and Cicirata, F. (2007) *Neuroscience* **148,** 653–667
23. Ambrosi, C., Boassa, D., Pranskevich, J., Smock, A., Oshima, A., Xu, J., Nicholson, B. J., and Sosinsky, G. E. (2010) *Biophys. J.* **98,** 1809–1819
24. Kneller, D. G., Cohen, F. E., and Langridge, R. (1990) *J. Mol. Biol.* **214,** 171–182
25. Garnier, J., Gibrat, J. F., and Robson, B. (1996) *Methods Enzymol.* **266,** 540–553
26. Cheng, J., Randall, A. Z., Sweredoski, M. J., and Baldi, P. (2005) *Nucleic Acids Res.* **33,** W72–76
27. Bryson, K., McGuffin, L. J., Marsden, R. L., Ward, J. J., Sodhi, J. S., and Jones, D. T. (2005) *Nucleic Acids Res.* **33,** W36–W38
28. Cole, C., Barber, J. D., and Barton, G. J. (2008) *Nucleic Acids Res.* **36,** W197–W201
29. Hand, G. M., Müller, D. J., Nicholson, B. J., Engel, A., and Sosinsky, G. E. (2002) *J. Mol. Biol.* **315,** 587–600
30. Oshima, A., Doi, T., Mitsuoka, K., Maeda, S., and Fujiyoshi, Y. (2003) *J. Biol. Chem.* **278,** 1807–1816
31. Oshima, A., Tani, K., Hiroaki, Y., Fujiyoshi, Y., and Sosinsky, G. E. (2007) *Proc. Natl. Acad. Sci. U.S.A.* **104,** 10034–10039
32. Tang, G., Peng, L., Baldwin, P. R., Mann, D. S., Jiang, W., Rees, I., and Ludtke, S. J. (2007) *J. Struct. Biol.* **157,** 38–46
33. Ramundo-Orlando, A., Serafino, A., Schiavo, R., Liberti, M., and d'Inzeo, G. (2005) *Biochim. Biophys. Acta* **1668,** 33–40
34. Díez, J. A., and Villalobo, A. (1996) in *Handbook of Nonmedical Applications of Liposomes* (Barenholz, Y., and Lasic, D. D. eds) pp. 261–270, CRC Press, Boca Raton, FL
35. Gooden, M., Rintoul, D., Takehana, M., and Takemoto, L. (1985) *Biochem. Biophys. Res. Commun.* **128,** 993–999
36. Locke, D., Koreen, I. V., Liu, J. Y., and Harris, A. L. (2004) *J. Biol. Chem.* **279,** 22883–22892
37. Wang, J., Ma, M., Locovei, S., Keane, R. W., and Dahl, G. (2007) *Am. J. Physiol. Cell Physiol* **293,** C1112–C1119
38. Locovei, S., Wang, J., and Dahl, G. (2006) *FEBS Lett.* **580,** 239–244
39. Li, X., Su, V., Kurata, W. E., Jin, C., and Lau, A. F. (2008) *J. Biol. Chem.* **283,** 5748–5759
40. Iglesias, R., Dahl, G., Qiu, F., Spray, D. C., and Scemes, E. (2009) *J. Neurosci.* **29,** 7092–7097
41. Maeda, S., Nakagawa, S., Suga, M., Yamashita, E., Oshima, A., Fujiyoshi, Y., and Tsukihara, T. (2009) *Nature* **458,** 597–602
42. Southworth, D. R., and Agard, D. A. (2008) *Mol. Cell* **32,** 631–640
43. Lai, C. P., Bechberger, J. F., and Naus, C. C. (2009) *Oncogene* **28,** 4402–4408
44. Boassa, D., Qiu, F., Dahl, G., and Sosinsky, G. (2008) *Cell Commun. Adhes.* **15,** 119–132
45. Stebbings, L. A., Todman, M. G., Phelan, P., Bacon, J. P., and Davies, J. A. (2000) *Mol. Biol. Cell* **11,** 2459–2470
46. Bunse, S., Locovei, S., Schmidt, M., Qiu, F., Zoidl, G., Dahl, G., and Dermietzel, R. (2009) *FEBS J.* **276,** 6258–6270